The Cryosphere Discuss., 8, 479–508, 2014
www.the-cryosphere-discuss.net/8/479/2014/
doi:10.5194/tcd-8-479-2014

The Cryosphere Discussions
Open Access

Dynamic response of Antarctic ice shelves to bedrock uncertainty

S. Sun[1], S. L. Cornford[2], Y. Liu[1], and J. C. Moore[1,3,4]

[1]College of Global Change and Earth Systerm Science, Beijing Normal University, Beijing, China
[2]School of Geographical Sciences, University of Bristol, Bristol BS8 1SS, UK
[3]Arctic Centre, University of Lapland, PL122, 96100 Rovaniemi, Finland
[4]Department of Earth Sciences, Uppsala University, Villavägen 16, Uppsala, 75236, Sweden

Received: 2 January 2014 – Accepted: 8 January 2014 – Published: 21 January 2014

Correspondence to: J. C. Moore (john.moore.bnu@gmail.com)

Published by Copernicus Publications on behalf of the European Geosciences Union.

Abstract

Bedrock geometry is an essential boundary condition in ice sheet modelling. The shape of the bedrock on fine scales can influences ice sheet evolution, for example through the formation of pinning points that alter grounding line dynamics. Here we test the sensitivity of the BISICLES adaptive mesh ice sheet model to small amplitude height fluctuations on different spatial scales in the bed rock topography provided by bedmap2 in the catchments of Pine Island Glacier, the Amery Ice Shelf, and a region of East Antarctica including the Denman and Totten Glaciers. We generate an ensemble of bedrock topographies by adding random noise to the bedmap2 data with amplitude determined by the accompanying estimates of bedrock uncertainty. Lower frequency coherent noise, which generates broad spatial scale (over 10s of km) errors in topography with relatively gently slopes, while higher frequency noise has steeper slopes over smaller spatial scales. We find that the small amplitude fluctuations result in only minor changes in the way these glaciers evolve. However, lower frequency noise is more important than higher frequency noise even when the features have the same height amplitudes and the total noise power is maintained. This provides optimism for credible sea level rise estimates with presently achievable densities of thickness measurements. Pine Island Glacier appears to be the most sensitive to errors in bed topography, while Lambert–Amery is stable under the present day observational data uncertainty. Totten–Denman region may undergo a retreat around Totten ice shelf, where the bedrock is lower than the sea level, especially if basal melt rates increase.

1 Introduction

Future mass loss from Antarctica is the most significant unknown part of the global sea level budget (Moore et al., 2013). Almost all the snow that falls on Antarctica is carried by ice flow from the continent where it either calves as icebergs or is removed by basal melting underneath ice shelves and floating glacier tongues (Rignot et al.,

TCD
8, 479–508, 2014

2008; Rignot et al., 2013). Ice shelves play an important role in the mass balance of the Antarctic ice sheet through their buttressing effect on the grounded ice sheet (Pritchard et al., 2012). Modification of back stress across the grounding line due to ice shelf grounded locations or embayments will hence impact sea level rise. Antarctica lost about 1350 ± 1010 Gt of grounded ice between 1992 and 2011 (Shepherd et al., 2012), equivalent to an increase in global mean sea level of 4.0 ± 3.0 mm. Both calving and basal melting of ice shelves are processes which are challenging to incorporate into ice dynamics models (Moore et al., 2013).

Using high precision remote sensing observations (e.g. Wingham et al., 1998, 2006; Rignot and Thomas, 2002; Zwally et al., 2005; Velicogna and Wahr, 2006; Dutrieux et al., 2013; Sasgen et al., 2013), estimates of ice sheet mass balance can be made. For East Antarctica, the ice sheet is close to balance (Rignot et al., 2008; Shepherd and Wingham, 2007; Shepherd et al., 2012). However, regionally ice shelves differ, with net ice loss in some glaciers in Wilkes Land and gain in Filchner and Ross ice shelves (Rignot et al., 2008). West Antarctica has long been known to be responsible for most of the negative Antarctic mass balance (Wingham et al., 2006). For example, Pine Island Glacier lost about 101.2±8 Gt yr^{-1} between the year 2003 and 2008 (Rignot et al., 2013).

Bedrock topography is an important parameter when simulating the ice sheet evolution. Many Antarctic phenomena are tightly controlled by the bedrock topography, such as the surface undulations ice streams (De Rydt et al., 2013), grounding line retreat (Favier et al., 2012), and tidewater outlet glaciers dynamics (Enderlin et al., 2013). Calving is also related to damage caused by ice flow over basal obstacles upstream of the grounding line or lateral shearing along nunataks or stagnant ice (Albrecht and Levermann, 2012) and basal melting is affected by the geometry of the sub-ice shelf cavity, particularly near the grounding line (Jacobs et al., 2011; Timmermann et al., 2012).

In West Antarctica, the reverse sloping bedrock has long been a focus as it was thought could lead to positive feedback between ice flux and retreating grounding line, since the ice flux has positive relationship with the ice thickness. However this hypothesis is debatable (Gudmundsson et al., 2012) since stable grounding line positions have been shown to occur in more complex three dimensional models. Pinning points beneath an ice shelf have a stabilising effect on the ice dynamics (Favier et al., 2012), and Durand et al. (2011) used a Full Stokes 2-dimension model to test the sensitivity of an ice sheet lying on a reverse bedrock slope to varying hill and trough geometry close to the grounding line. In reality, because of the difficulty in observing the sub-ice sheet bedrock elevation, bedrock topography will always have uncertainties.

Bedrock topography has been observed primarily by radar sounding in the megahertz frequency range (e.g. Robin et al., 1969), with bandwidths and hence vertical resolutions in the 10 metre range. Seismic surveys have also been particularly useful on ice shelves (Pozdeev and Kurinin, 1987) where the presence of slightly saline marine ice layers may prevent penetration of radar waves (Moore et al., 1994), and sea water prevents mapping of the sub-shelf cavity. The amplitude of the ice thickness uncertainty in mapped topography will vary both along the radar flight line as a result of the bandwidth of the radar used, and in between flight lines as a result of the mapping interpolation algorithms selected. The spacing between flight lines is seldom less than some kilometres and over much of Antarctica may be considerably larger (Fretwell et al., 2013). Besides the large amplitude fluctuations such as produced by hills and valleys, the small amplitude errors in elevation or irregularities in the bed may affect ice sheet evolution. For example the differences in surface roughness or fractal dimension between a hard rock bed substrate and a fine sedimentary deposit will not be directly visible using radars presently designed to map ice sheet thickness. To date no research on the impact of these small amplitude bedrock fluctuations on real glacier with three dimensional topography has been made. However, Durand et al. (2011) used a 2-dimensional Full-Stokes model on a synthetic Pine Island-like flowline geometry and found that, if bedrock that was over-smoothed, then a large bias of up to 25 % in ice volume in the basin could occur.

TCD
8, 479–508, 2014

In ice sheet modelling, the data used are often smoothed to allow representation in continuum models which require continuous spatial derivatives to exist. In reality, there will be small amplitude fluctuations making the bedrock rougher. The density of ice thickness measurements determines the amplitude of the fluctuations that may exist in each location – and this has a standard deviation from 50 m to about 1 km. We call these uncertainties noise, and want to test the sensitivity of Antarctic ice sheet to this bedrock noise. We wish here to quantify various issues: will the bedrock noise affect the evolution of the ice sheet, such as grounding line retreat and mass balance change, and how? How much can we trust our modelling result? Which kind of noise has larger influence to the glacier, lower frequency or higher frequency? Since the bedrock features are quite different between East and West Antarctica, how do their ice sheets respond to the same kind of noise?

To answer these questions, we make sensitivity experiments with bedrock noise on three basins, Pine Island bay, Lambert–Amery system and Totten–Denman region (Fig. 1). Pine Island Glacier (PIG) is the archetypical glacier of a vulnerable West Antarctic ice sheet, lying on reverse sloping bedrock below the sea level (Fig. 2a) with its grounding line retreating rapidly at present. Most of the Lambert basin is a.s.l., with a deep trough however beneath the Amery ice shelf (Fig. 2b). The mass balance of this system is estimated to be close to zero but with large uncertainty. The bedrock of Totten–Denman region is flat and close to sea level with a deep trough beneath Totten glacier, which is the largest ice discharger in East Antarctica (Fig. 2c). Ice mass loss from the region is via Totten (Fig. 2f) and other ice shelves that fringe the coast line. We add noise of three different spectral frequencies on the bedrock maps of these glaciers, and make a simulation for 200 yr to make a noise sensitivity analysis.

In Sect. 2, we introduce the methodology of tuning the model and making the noisy bedrock input data. In Sect. 3, we show the results of the three different glacier outcomes responding to different frequency bedrock noise and discuss the results and implications in Sect. 4.

TCD
8, 479–508, 2014

2 Methods

The influence of bedrock on ice sheet evolution is usually considered using large amplitude positive and negative change in slope such as a hill or a valley (Durand et al., 2011). Since we want to simulate more realistic situations, we chose to consider the small amplitude noise distributed according to the uncertainty map of bedrock topography. We made three varieties of red noise by frequency: higher, medium, and lower. To explore statistical variability, we use 50 different realizations of topography disturbed by initially white Gaussian noise transformed for each frequency range of noise.

2.1 Producing noisy data

Our model was initialized using the best available bedrock topography. For PIG, we simulate a $512 \times 512\,\mathrm{km}^2$ area, using a 1 km resolution DEM (1996 datum) constructed along the same lines as the 5 km ALBMAP DEM (Le Brocq et al., 2010), which differs by only tens of meters from the same region on bedmap2 (Fretwell et al., 2013). For the Lambert–Amery system ($1536 \times 1536\,\mathrm{km}^2$ domain) and Totten–Denman region ($1792 \times 1792\,\mathrm{km}^2$ domain), we use the bedmap2 geometry data (Fretwell et al., 2013).

In signal processing, white noise is a random signal with a flat power spectral density. We ensure that the power within any frequency band of fixed width is the same. White noise generated using a random uniform probability distribution is arranged in rectangular grids (Fig. 3a).

First, we create 2-dimensional white noise on the domain we modelled, named $f(x,y)$, where x and y are the domain coordinate. PIG domain has 512 grid cells in both x and y directions, so the value ranges of x and y are both 1–512. Since we want to test the ice sheet sensitivity to the frequency of bedrock noise, we have to create noise of high frequency and low frequency. We transform our noise $f(x,y)$ from the spatial domain to frequency domain through the 2-dimensional discrete Fourier transform. Assume the noise on the frequency domain is $F(u,v)$, then $f(x,y)$ and $F(u,v)$

have relationship as followed.

$$F(u,v) = \sum_{x=0}^{N-1}\sum_{y=0}^{N-1} f(x,y)e^{-i2\pi\left(\frac{ux}{m}+\frac{vy}{N}\right)} \quad (1)$$

Where $0 \leq u \leq M-1, \quad 0 \leq v \leq N-1$.

M and N are the number of grid nodes in the x and y directions, and here for all three of our sites $M = N$. Then we rearrange the outputs by moving the zero-frequency component to the centre of the array. The Gaussian lower pass filter has the following form:

$$H(u,v) = e^{-\left[\left(u-\frac{M}{2}\right)^2+\left(v-\frac{N}{2}\right)\right]/2\sigma^2} \quad (2)$$

After filtering by the Gaussian lower pass filter (in other words, by the function $F(u,v)\cdot H(u,v)$), the original white noise has been mapped to noise with frequency distribution determined by the isotropic standard deviation σ. We chose $\sigma = 10$, 50, 100 (units: $1/M$ cycles km^{-1}) to generate lower, medium, higher frequency noise (Fig. 3). We then transform the noise back to the spatial domain as

$$f(x,y) = \frac{1}{MN}\sum_{u=0}^{N-1}\sum_{v=0}^{N-1} F(u,v)\cdot H(u,v)e^{-i2\pi\left(\frac{ux}{m}+\frac{vy}{N}\right)} \quad (3)$$

When filtering the noise, we tune the power of the white noise to keep the lower, medium, and higher frequency noise at the same power. For PIG, which has the most dense coverage of radar, errors are more or less constant over the whole region and most of the noise values are in the range [−60, 60] m. Figure 3e–g shows the effects of the three noise distributions on the bedrock height noise patterns. Since the amplitude of variation is determined by the uncertainty in the observations, in reality the lowest frequency pattern may mimic the effects of coherent bias in errors producing broad features with gentle slopes on special scales of 10s of km (Fig. 3e). The medium

(Fig. 3f) and high (Fig. 3g) frequency noise patterns vary over smaller spatial scales and can represent moderately sloping surface undulations or rough terrain down to sub-kilometre scales. For the two other regions we study, the bedrock mapping uncertainty varies spatially, and so the noise amplitudes are designed to vary spatially also, but we still can define the noise distributions in frequency space as for the PIG example in Fig. 3b–d.

For the East Antarctic Ice Sheet, the uncertainty of bedrock elevation data ranges from 66 m to more than 1000 m, so we use different noise ranges according to the local data uncertainty (Fretwell et al., 2013). As is shown in Fig. 4a and c, there are topographic uncertainties with 16 different values across different domains. We combined closest values such as (151, 152, 154 m) into a class where the uncertainties lie in the intervals [66, 100], [100, 180], [180, 238], [238, 500] and [500, 1008] m. In each of these areas, we created maps of noise with the standard deviation around 88, 150, 200, 300 and 1000 m, and then we combined these noise sets to create a map spanning the model domain (Fig. 4b and d).

After making the bedrock noise, we add it to the bedrock map beneath the grounded ice sheet and subtract the same value from ice sheet thickness to keep the surface elevation consistent with the geometry data.

To summarize, a Gaussian low pass filter is used to select noise with three different frequency distributions but with the same power. The resulting noise maps are added on the bedrock to provide a set of perturbed geometries. We then use these geometries we made to initialize the ice sheet model.

2.2 Model

The ice sheet model we used for the simulation is BISICLES (Cornford et al., 2013). The model use a vertically-integrated treatment of the momentum equation based on L1L2, (Schoof and Hindmarsh, 2010). This physical mechanism is quite suitable for ice shelves and fast flowing ice streams. It is a high-performance scalable AMR (Adaptive Mesh Refinement) ice sheet model constructed using the Chombo parallel AMR

TCD
8, 479–508, 2014

framework, which allows us to use non-uniform, evolving meshes. Here we implement a mesh with 3 levels of refinement on top of a 4 km resolution coarse mesh. The resolution of the vast slow flowing area is 4 km, while the highest resolution of the fast flowing area and grounding line is 0.5 km. Meshes are generated at each time step. Linear interpolation is used to determine variable values where the mesh is newly refined, and arithmetic averaging is used in regions where the mesh is coarsened. Specified numerical treatment on the multigrid mesh can be found in Cornford et al. (2013). The high resolution mesh area evolves with changes in the location of the grounding line and the ice streams. In this way, we can capture the dynamics of grounding line and ice streams without wasting computational resources. We run 200 yr long prognostic simulations with perturbation on the bedrock being the only difference between ensemble members. For PIG, each of the 50 simulations required one day, while the larger Lambert–Amery domain needed 3 days, and the Totten–Denman region 5 days per simulation with a 16 core processor. The computing time was bedrock dependent and simulations with higher frequency noise took longer to achieve convergence.

For each ice sheet, we add lower, medium and higher frequency noise on the bedrock. For each kind of frequency, we made 50 sets of noise as described in Sect. 2.1. The basal traction coefficient is calculated using a control method similar to those reported in Joughin et al. (2009, 2010); MacAyeal (1993) and Morlighem et al. (2010), that is, a gradient based optimization method which makes use of the model adjoint equations. The target surface velocities were acquired during the 2007/8 international polar year (Rignot et al., 2011), and ice temperatures from a 5 km grid computed by Pattyn (2010). We use surface mass balance estimates from Arthern et al. (2006).

The sub-ice shelf melting can be determined indirectly from estimates of ice shelf mass balance (e.g., Rignot et al., 2008; Pritchard et al., 2012). To simplify the parameterization we assume that melt is highest at the grounding line where one might expect deeper and warmer water. We imposed as a piecewise linear melt as a function of the ice shelf thickness (Cornford et al., 2013). For Pine Island Glacier, we use a maximum

TCD
8, 479–508, 2014

melting rate of 50 $m\,yr^{-1}$ (Joughin et al., 2010; Payne et al., 2006; Jacobs et al., 2011) where ice is thicker than 500 m, linearly decreasing to no melt where ice is thinner than 50 m. For the East Antarctica Lambert–Amery system, the melt rate around the grounding line was determined to be about 30 $m\,yr^{-1}$ (Rignot et al., 2002; Wen et al., 2010) so we use this value where ice is thicker than 1500 m, linearly decreasing to no melt where ice is thinner than 300 m. For Totten and Moscow ice shelves, temperatures at the deep grounding line are more than 3 °C above melting point and the ice shelves are considered to be retreating (Rignot et al., 2013). We constrain melting rates such that the grounding line retreats and the whole basin mass loss comparable to that found by Rignot et al. (2008). Hence we choose a high maximum melt rate of 90 $m\,yr^{-1}$ where ice is thicker than 1500 m, linearly decreasing to no melt where ice is thinner than 300 m. The simple parameterization used here does not allow for basal accretion of marine ice under ice shelves – known to occur, for example under parts of the Amery ice shelf (Fricker et al., 2001). However, while the melt rates are not realistic in all respects, they do allow the model to produce behaviour consistent with observations.

3 Results

In this section, we present the model results for the Pine Island Glacier, Lambert–Amery system and Totten–Denman region simulations running for 200 yr and essentially representing the basin evolution from the year 2000 to 2200. We also run a control experiment where no noise is added to the topography as described in the published bedrock topographic maps.

3.1 Pine Island Glacier

The ice volume above flotation (VAF) reduces during the simulation period. The result with lower frequency noise on the bedrock has the largest standard deviation (Fig. 5).

TCD
8, 479–508, 2014

We also calculate the retreating rate year by year (Fig. 6). The retreating rate is around 0.1 mm yr^{-1} sea level rise equivalent per year at the first years, and then rises abruptly to 0.25 mm yr^{-1} after around the 50th year.

The grounding line also shows a large retreat from about the 50th year, so we label this year the onset of retreat. For the experiment with lowest frequency noise on the bedrock, the onset of retreat ranges from the 41st year to the 76th year. With medium frequency noise, the onset ranges from the 48th year to the 64th year and for the highest frequency noise, the onset ranges from the 46th year to the 59th year. The scatter of the retreating year is lower as the frequency of noise adding on the bedrock is raised.

In our simulation, the grounding line will retreat by more than 100 km (Fig. 2d, Fig. 7) during the simulation time. The grounding line locations at the last simulation year are also influenced (Fig. 7). For the experiment with lowest frequency noise on the bedrock, the most northerly locations of grounding differ by as much as 53 km. For medium frequency noise, the value is 25 km and with highest frequency noise, the value reduces to 20 km. This variability is dominated by the variations in the onset of retreat, as the rates of retreat after onset are similar in all cases.

3.2 Lambert–Amery System

To see the VAF fluctuation caused by the dynamics, we made a fast flowing mask (ice velocity > 100 m yr^{-1}) on the whole system (Fig. 8). The fast flowing area (mainly Amery ice shelf) is quite stable compared with PIG and there is no overall trend of grounding line retreat or advance (Fig. 2e, Fig. 8). We calculate the VAF and retreating rate (sea level rise equivalence) per year of the whole Lambert–Amery system, and the fast flow area separately (Fig. 9). The VAF for the whole basin is increased with a similar linear trend, which is controlled by the ice mass accumulation every year.

After adding noise on the bedrock, the mean value of VAF is higher than for the noiseless control experiment, since after we added the noise, some floating areas become grounded. The standard deviation of ice volume above floatation is smaller for experiments with higher frequency noise on the bedrock than the low frequency one. The retreating rate is quite similar using different noisy bedrock, near to zero sea level rise equivalence (Fig. 9). The most southern location of the grounding line will retreat about 10 km during the simulation time (Figs. 2e and 8). For every experiment with any kind of noise, the location of the grounding lines at the last simulating year is much the same as in the noiseless simulation (Fig. 8).

3.3 Totten–Denman Region

The VAF reduces during the simulation period. The result with lowest frequency noise on the bedrock has the largest standard deviation. The retreating rate increases during the first 50 yr and then decrease to around zero. The retreating rates are much the same with all three frequencies of noise on the bedrock (Fig. 10).

In the simulation of this region, the grounding line retreated furthest (about 80 km) where the bedrock is below sea level, such as Totten ice shelf and Moscow University ice shelf (Fig. 11b). The ice grounded on the trough in the east of Totten may begin to float forming an ice shelf between Wilkes Land and Law Dome in the noiseless simulation. However, uncertainty of grounding line location means that it is not certain that Law Dome will become an island detached from the mainland. The uncertainty in grounding line is larger for lowest frequency noise experiment than for the highest frequency noise experiment, but the difference is small (Fig. 11c–e). The grounding line is stable in most of regions but advances near the Denman ice shelf where bedrock is obviously above sea level (Fig. 11a). The combination of advancing and retreating grounding line leads to the less net contribution to sea level than may be expected from only examining the Totten region.

TCD
8, 479–508, 2014

4 Discussion and conclusion

The results of our simulations suggest that the low frequency noise on the bedrock plays a more important role on the ice sheet retreat than high frequency noise. This suggests that a small number of more spatially coherent bedrock irregularities represented by the lowest frequency noise examples we show, are more important than small scale surface roughness. Since radar is intrinsically limited in detecting small amplitude features by bandwidth and the spatial resolution is limited by diffraction effects, higher frequency errors in topography would likely remain undetected. However the low frequency features should be detectable if the density of measurements is large enough. This is reassuring for our confidence in estimating ice sheet behaviour using measurements at high spatial resolution across critical zones such as the grounding line. Durand et al. (2011) found that spatial resolutions as high a 1 km were needed to prevent large fluctuations of the grounding line in a flow line model due to oversmoothing of bedrock. Their bedrock topography was based on sampling a fractal bed at different resolutions, whereas ours is based on red noise with specified amplitude and total power set to Bedmap2 observational uncertainties by design. Perhaps the more important difference between our simulations and the Durand et al. (2011) flow line study is in the extension to a two-dimensional bedrock where buttressing effects can stabilize reverse sloping beds across the ice flow direction (Gudmundsson et al., 2012; Gudmundsson, 2013).

The onset of retreat at Pine Island Glacier is affected by bed uncertainty. The glacier undergoes a step change in rates of mass loss when the grounding line retreats across to the reverse slope. After adding noise on the bedrock, the onset of retreat is advanced or delayed. The low frequency noise in our experiment creates a 35 yr uncertainty while the high frequency noise leads to about 14 yr uncertainty on the onset of retreat. Both Lambert–Amery system and Totten–Denman region do not have such a step change in rate of mass loss.

TCD
8, 479–508, 2014

We use the change of ice volume above flotation equivalent to sea level rise per year to evaluate the retreating rate. We find that the noise added on the bedrock does not change the retreating rate greatly in any of the three regions we simulated. So we think that although there are uncertainties of the observation data, that uncertainty will not lead to conspicuous differences in the retreating rate.

The activity of the grounding line is quite different between the three ice sheet regions we examined with relatively fast retreat beneath the Pine Island Glacier compared with the other two regions. The locations of the grounding line varies a lot in the last simulation year (about AD 2200) for Pine Island Glacier, while the variability in position for Lambert–Amery system and Totten–Denman region are relatively small. In these simulations we have not considered changes in the relative sea level associated with changing mean sea level or local lithospheric loading by the ice sheet. This will be a factor in grounding line location especially in long term ice sheet mass change (Moore et al., 2013), and the elastic response is known to be measurable when ice shelves disintegrate rapidly (Thomas et al., 2011).

The parameterization of sub shelf melt rates we use is simplistic, but does lead to behaviour consistent with present behaviour of the ice shelves and grounding lines. It is plausible that changes in melt rate could occur if the relatively warm circumpolar Antarctic deep waters starts to track closer to the continent (Pritchard et al., 2012), perhaps as a response to changing global temperatures (Moore et al., 2013). Under such conditions the geometry of the sub shelf cavity and the proximity of the continental shelf break will be important to the ice shelf stability. The expected loss of grounded ice in the trough between Law Dome and Wilkes Land may not, in future, be occupied by an ice shelf but rather by an open water strait given the high melt rates at present under Totten ice shelf, its northerly location and the proximity of relatively warm waters. All in all, the retreating rate is not very sensitive to present day observational bedrock data uncertainty. However, more caution should be taken when simulating the Pine Island Glacier, or even the whole West Antarctica with such retrograde bedrock, especially with reference to the grounding line evolution. Lambert–Amery is stable under the present day observation data uncertainty. Totten–Denman region may undergo a retreat around Totten ice shelf where the bedrock is lower than the sea level, and Law Dome become an island perhaps connected via an ice shelf to the main land in the warm future.

Acknowledgements. Funding came from NSFC No. 41076125, NBRPC 2012CB957704; Fundamental Research Funds for the Central Universities of China 2013NT53, and is publication number 35 of the Nordic Centre of Excellence SVALI, Stability and Variations of Arctic Land Ice funded by the Nordic Top-level Research Initiative.

References

Albrecht, T. and Levermann, A.: Fracture field for large-scale ice dynamics, J. Glaciol., 58, 165–176, doi:10.3189/2012JoG11J191, 2012.

Arthern, R. J., Winebrenner, D. P., and Vaughan, D. G.: Antarctic snow accumulation mapped using polarization of 4.3 cm wavelength microwave emission, J. Geophys. Res.-Atmos., 111, D06107, doi:10.1029/2004JD005667, 2006.

Cornford, S. L., Martin, D. F., Graves, D. T., Ranken, D. F., Le Brocq, A. M., Gladstone, R. M., Payne, A. J., Ng, E. G., and Lipscomb, W. H.: Adaptive mesh, finite volume modeling of marine ice sheets, J. Comput. Phys., 232, 529–549, 2013.

De Rydt, J., Gudmundsson, G. H., Corr, H. F. J., and Christoffersen, P.: Surface undulations of Antarctic ice streams tightly controlled by bedrock topography, The Cryosphere, 7, 407–417, doi:10.5194/tc-7-407-2013, 2013.

Durand, G., Gagliardini, O., Favier, L., Zwinger, T., and le Meur, E.: Impact of bedrock description on modeling ice sheet dynamics, Geophys. Res. Lett., 38, L20501, doi:10.1029/2011GL048892, 2011.

Dutrieux, P., Vaughan, D. G., Corr, H. F. J., Jenkins, A., Holland, P. R., Joughin, I., and Fleming, A. H.: Pine Island glacier ice shelf melt distributed at kilometre scales, The Cryosphere, 7, 1543–1555, doi:10.5194/tc-7-1543-2013, 2013.

Enderlin, E. M., Howat, I. M., and Vieli, A.: High sensitivity of tidewater outlet glacier dynamics to shape, The Cryosphere, 7, 1007–1015, doi:10.5194/tc-7-1007-2013, 2013.

Favier, L., Gagliardini, O., Durand, G., and Zwinger, T.: A three-dimensional full Stokes model of the grounding line dynamics: effect of a pinning point beneath the ice shelf, The Cryosphere, 6, 101–112, doi:10.5194/tc-6-101-2012, 2012.

Fretwell, P., Pritchard, H. D., Vaughan, D. G., Bamber, J. L., Barrand, N. E., Bell, R., Bianchi, C., Bingham, R. G., Blankenship, D. D., Casassa, G., Catania, G., Callens, D., Conway, H., Cook, A. J., Corr, H. F. J., Damaske, D., Damm, V., Ferraccioli, F., Forsberg, R., Fujita, S., Gim, Y., Gogineni, P., Griggs, J. A., Hindmarsh, R. C. A., Holmlund, P., Holt, J. W., Jacobel, R. W., Jenkins, A., Jokat, W., Jordan, T., King, E. C., Kohler, J., Krabill, W., Riger-Kusk, M., Langley, K. A., Leitchenkov, G., Leuschen, C., Luyendyk, B. P., Matsuoka, K., Mouginot, J., Nitsche, F. O., Nogi, Y., Nost, O. A., Popov, S. V., Rignot, E., Rippin, D. M., Rivera, A., Roberts, J., Ross, N., Siegert, M. J., Smith, A. M., Steinhage, D., Studinger, M., Sun, B., Tinto, B. K., Welch, B. C., Wilson, D., Young, D. A., Xiangbin, C., and Zirizzotti, A.: Bedmap2: improved ice bed, surface and thickness datasets for Antarctica, The Cryosphere, 7, 375–393, doi:10.5194/tc-7-375-2013, 2013.

Gudmundsson, G. H., Krug, J., Durand, G., Favier, L., and Gagliardini, O.: The stability of grounding lines on retrograde slopes, The Cryosphere, 6, 1497–1505, doi:10.5194/tc-6-1497-2012, 2012.

Gudmundsson, G. H.: Ice-shelf buttressing and the stability of marine ice sheets, The Cryosphere, 7, 647–655, doi:10.5194/tc-7-647-2013, 2013.

Jacobs, S. S., Jenkins, A., Giulivi, C. F., and Dutrieux, P.: Stronger ocean circulation and increased melting under Pine Island Glacier ice shelf, Nat. Geosci., 4, 519–523, 2011.

Jenkins, A., Dutrieux, P., Jacobs, S. S., McPhail, S. D., Perrett, J. R., Webb, A. T., and White, D.: Observations beneath Pine Island Glacier in West Antarctica and implications for its retreat, Nat. Geosci., 3, 468–472, 2010.

Joughin, I., Tulaczyk, S., Bamber, J. L., Blankenship, D., Holt, J. W., Scambos, T., and Vaughan, D. G.: Basal conditions for Pine Island and Thwaites Glaciers, West Antarctica, determined using satellite and airborne data, J. Glaciol., 55, 245–257, doi:10.3189/002214309788608705, 2009.

Joughin, I., Smith, B. E., and Holland, D. M.: Sensitivity of 21st century sea level to ocean-induced thinning of Pine Island Glacier, Antarctica, Geophys. Res. Lett., 37, L20502, doi:10.1029/2010GL044819, 2010.

Le Brocq, A. M., Payne, A. J., and Vieli, A.: An improved Antarctic dataset for high resolution numerical ice sheet models (ALBMAP v1), Earth Syst. Sci. Data, 2, 247–260, doi:10.5194/essd-2-247-2010, 2010.

MacAyeal, D. R.: A tutorial on the use of control methods in ice-sheet modeling, J. Glaciol., 39, 39–91, 1993.

Moore, J. C., Reid, A. P., and Kipfstuhl, J.: Microstructure and electrical properties of marine ice and its relationship to meteoric ice and sea ice, J. Geophys. Res.-Oceans, 99, 5171–5180, doi:10.1029/93JC02832, 1994.

Moore, J. C., Grinsted, A., Zwinger, T., and Jevrejeva, S.: Semiempirical and process-based global sea level projections, Rev. Geophys., 51, 484–522, doi:10.1002/rog.20015, 2013.

Morlighem, M., Rignot, E., Seroussi, H., Larour, E., Ben Dhia, H., and Aubry, D.: Spatial patterns of basal drag inferred using control methods from a Full-Stokes and simpler models for Pine Island Glacier, West Antarctica, Geophys. Res. Lett., 37, L14502, doi:10.1029/2010GL043853, 2010.

Pattyn, F.: Antarctic subglacial conditions inferred from a hybrid ice sheet/ice stream model, Earth Planet. Sc. Lett., 295, 451–461, 2010.

Payne, A. J., Holland, P. R., Shepherd, A. P., Rutt, I. C., Jenkins, A., and Joughin, I.: Numerical modeling of ocean-ice interactions under Pine Island Bay's ice shelf, J. Geophys. Res.-Oceans, 112, C10019, doi:10.1029/2006JC003733, 2007.

Pozdeev and Kurinin: New data on ice sheet morphology, bedrock and bottom relief in the Southern Weddell Sea Basin, West Antarctica, Antarktika, doklady komissii, 26, 66–71, 1987

Pritchard, H. D., Ligtenberg, S. R. M., Fricker, H. A., Vaughan, D. G., van den Broeke, M. R., and Padman, L.: Antarctic ice-sheet loss driven by basal melting of ice shelves, Nature, 484, 502–505, 2012.

Rignot, E.: Changes in West Antarctic ice stream dynamics observed with ALOS PALSAR data, Geophys. Res. Lett., 35, L12505, doi:10.1029/2008GL033365, 2008.

Rignot, E. and Jacobs, S. S.: Rapid bottom melting widespread near Antarctic ice sheet grounding lines, Science, 296, 2020–2023, doi:10.1126/science.1070942, 2002.

Rignot, E. and Thomas, R. H.: Mass Balance of Polar Ice Sheets, Science, 297, 1502–1506, doi:10.1126/science.1073888, 2002.

Rignot, E., Vaughan, D. G., Schmeltz, M., Dupont, T., and MacAyeal, D.: Acceleration of Pine Island and Thwaites Glaciers, West Antarctica, Ann. Glaciol., 34, 189–194, doi:10.3189/172756402781817950, 2002.

Rignot, E., Bamber, J. L., van den Broeke, M. R., Davis, C., Li, Y., van de Berg, W. J., and van Meijgaard, E.: Recent Antarctic ice mass loss from radar interferometry and regional climate modelling, Nat. Geosci., 1, 106–110, 2008.
Rignot, E., Mouginot, J., and Scheuchl, B.: Ice Flow of the Antarctic Ice Sheet, Science, 333, 1427–1430, doi:10.1126/science.1208336, 2011.
Rignot, E., Jacobs, S., Mouginot, J., and Scheuchl, B.: Ice-Shelf Melting Around Antarctica, Science, 341, 266–270, doi:10.1126/science.1235798, 2013.
Robin, G. D. Q., Evans, S., and Bailey, J. T.: Interpretation of radio echo sounding in polar ice sheets, Philos. T. R. Soc. Lond., 265, 437–505, doi:10.2307/73767TS3, 1969.
Sasgen, I., Konrad, H., Ivins, E. R., Van den Broeke, M. R., Bamber, J. L., Martinec, Z., and Klemann, V.: Antarctic ice-mass balance 2003 to 2012: regional reanalysis of GRACE satellite gravimetry measurements with improved estimate of glacial-isostatic adjustment based on GPS uplift rates, The Cryosphere, 7, 1499–1512, doi:10.5194/tc-7-1499-2013, 2013.
Scambos, T. A., Haran, T. M., Fahnestock, M. A., Painter, T. H., and Bohlander, J.: MODIS-based Mosaic of Antarctica (MOA) data sets: continent-wide surface morphology and snow grain size, Remote Sens. Environ., 111, 242–257, 2007.
Schoof, C.: Ice sheet grounding line dynamics: steady states, stability, and hysteresis, J. Geophys. Res.-Ea. Surf., 112, F03S28, doi:10.1029/2006JF000664, 2007.
Schoof, C. and Hindmarsh, R. C. A.: Thin-film flows with wall slip: an asymptotic analysis of higher order glacier flow models, Q. J. Mech. Appl. Math., 63, 73–114, doi:10.1093/qjmam/hbp025, 2010.
Shepherd, A. and Wingham, D.: Recent sea-level contributions of the Antarctic and Greenland ice sheets, Science, 315, 1529–1532, doi:10.1126/science.1136776, 2007.
Shepherd, A., Ivins, E. R., Geruo, A., Barletta, V. R., Bentley, M. J., Bettadpur, S., Briggs, K. H., Bromwich, D. H., Forsberg, R., Galin, N., Horwath, M., Jacobs, S., Joughin, I., King, M. A., Lenaerts, J. T. M., Li, J., Ligtenberg, S. R. M., Luckman, A., Luthcke, S. B., McMillan, M., Meister, R., Milne, G., Mouginot, J., Muir, A., Nicolas, J. P., Paden, J., Payne, A. J., Pritchard, H., Rignot, E., Rott, H., Sørensen, L. S., Scambos, T. A., Scheuchl, B., Schrama, E. J. O., Smith, B., Sundal, A. V., van Angelen, J. H., van de Berg, W. J., van den Broeke, M. R., Vaughan, D. G., Velicogna, I., Wahr, J., Whitehouse, P. L., Wingham, D. J., Yi, D., Young, D., and Zwally, H. J.: A reconciled estimate of ice-sheet mass balance, Science, 338, 1183–1189, doi:10.1126/science.1228102, 2012.

TCD
8, 479–508, 2014

Dynamic response of Antarctic ice shelves to bedrock uncertainty

S. Sun et al.

Thomas, I. D., King, M. A., Bentley, M. J., Whitehouse, P. L., Penna, N. T., Williams, S. D. P., Riva, R. E. M., Lavallee, D. A., Clarke, P. J., King, E. C., Hindmarsh, R. C. A., and Koivula, H.: Widespread low rates of Antarctic glacial isostatic adjustment revealed by GPS observations, Geophys. Res. Lett., 38, L22302, doi:10.1029/2011GL049277, 2011.

Timmermann, R., Wang, Q., and Hellmer, H. H.: Ice-shelf basal melting in a global finite-element sea-ice/ice-shelf/ocean model, Ann. Glaciol., 53, 303–314, doi:10.3189/2012AoG60A156, 2012.

Velicogna, I. and Wahr, J.: Measurements of time-variable gravity show mass loss in Antarctica, Science, 311, 1754–1756, doi:10.1126/science.1123785, 2006.

Wingham, D. J., Ridout, A. J., Scharroo, R., Arthern, R. J., and Shum, C. K.: Antarctic elevation change from 1992 to 1996, Science, 282, 456–458, doi:10.1126/science.282.5388.456, 1998.

Wingham, D. J., Shepherd, A., Muir, A., and Marshall, G. J.: Mass balance of the Antarctic ice sheet, Philos. T. R. Soc. A, 364, 1627–1635, doi:10.1098/rsta.2006.1792, 2006.

Wingham, D. J., Wallis, D. W., and Shepherd, A.: Spatial and temporal evolution of Pine Island glacier thinning, 1995–2006, Geophys. Res. Lett., 36, L17501, doi:10.1029/2009GL039126, 2009.

Zwally, H. J., Giovinetto, M. B., Li, J., Cornejo, H. G., Beckley, M. A., Brenner, A. C., Saba, J. L., and Yi, D.: Mass changes of the Greenland and Antarctic ice sheets and shelves and contributions to sea-level rise: 1992–2002, J. Glaciol., 51, 509–527, doi:10.3189/172756505781829007, 2005.

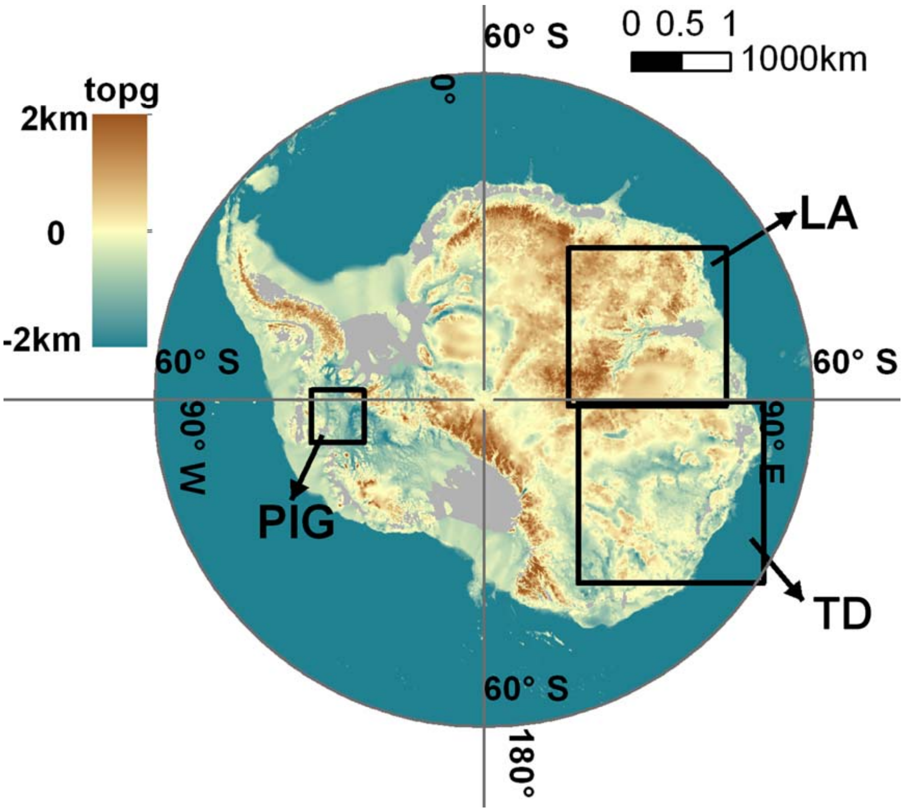

Fig. 1. The three basins (boxed) we simulated on the Bedmap2 Antarctic bedrock topography map (Fretwell et al., 2013). Pine Island Glacier (PIG) is shown in Fig. 2a, Lambert–Amery (LA) system is shown in Fig. 2b and Totten–Denman region (TD) is shown in Fig. 2c.

TCD
8, 479–508, 2014

Dynamic response of Antarctic ice shelves to bedrock uncertainty

S. Sun et al.

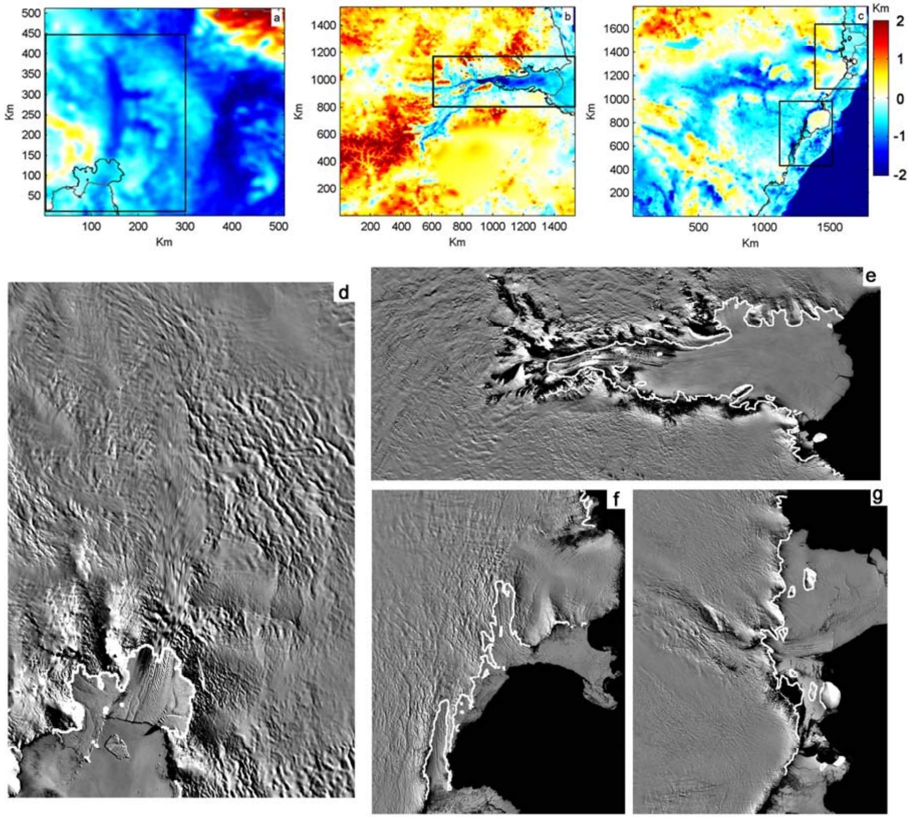

Fig. 2. Bedrock topography map for PIG (**a**; Le Brocq et al., 2010), LA (**b**; Fretwell et al., 2013), TD (**c**; Fretwell et al., 2013). Grounding lines are shown in black. **(d–g)** Are MODIS Mosaic of Antarctica(MOA) Image Map 2003–2004, (Scambos et al., 2007) of the corresponding boxed area in **(a–c)** with grounding lines shown in white.

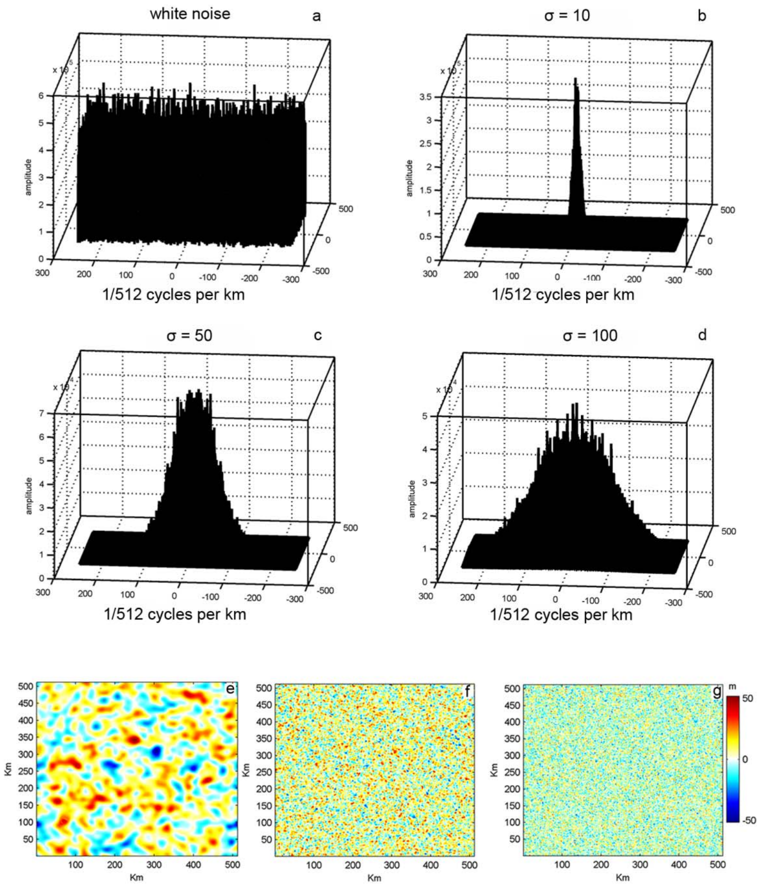

Fig. 3. (a–d) Noise spectrum for different distributions as labeled. The units of σ are: 1/512 cycles per km, and the total power in each noise realization is the same. **(e–g)** Are plots of the lower, medium, higher frequency noise added to the spatial domain of Pine Island Glacier (Fig. 2a).

TCD
8, 479–508, 2014

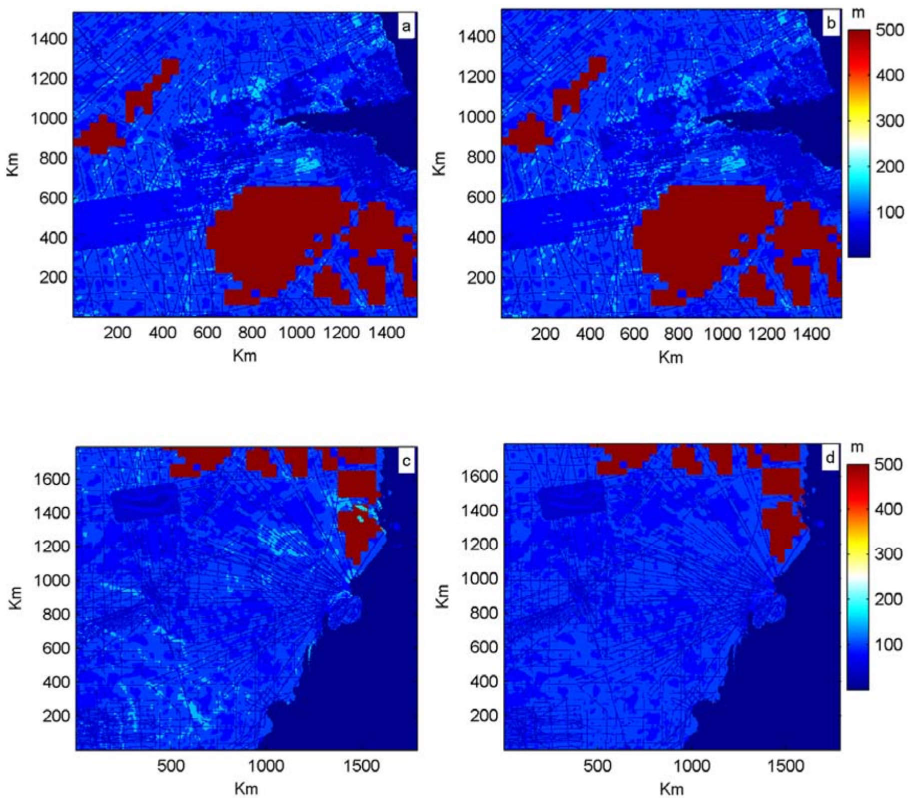

Fig. 4. Comparison of uncertainty maps from Bedmap2 (**a**, **c**; Fretwell et al., 2013) and the one we use in the model **(b, d)** for Lambert–Amery basin **(a, c)** and Totten–Denman region **(b, d)**. There are 16 single uncertainty values in bedmap2, we combined some close values and actually use 6 uncertainty values. For PIG the uncertainty was uniformly 60 m acorss the whole domain (Fig. 3e–g).

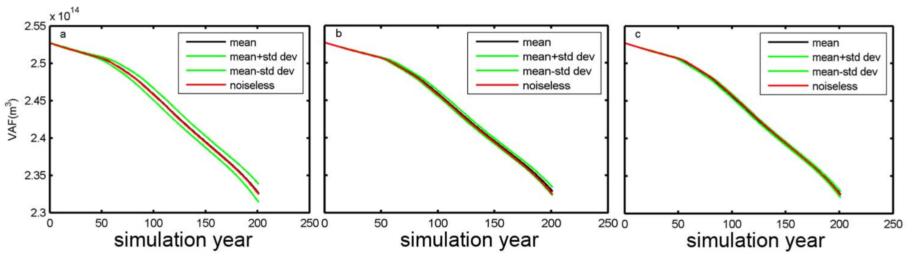

Fig. 5. Ice volume above floatation (VAF) in the PIG basin (Fig. 2a and d). The mean value of noisy experiments is very close to that of the noiseless experiment. The three columns are for experiments with lower **(a)**, medium **(b)** and higher **(c)** frequency noise on the bedrock. The red curve is for noiseless result, the black line is the mean value for each set of results and the green curve are mean VAF plus and minus one standard deviation.

TCD
8, 479–508, 2014

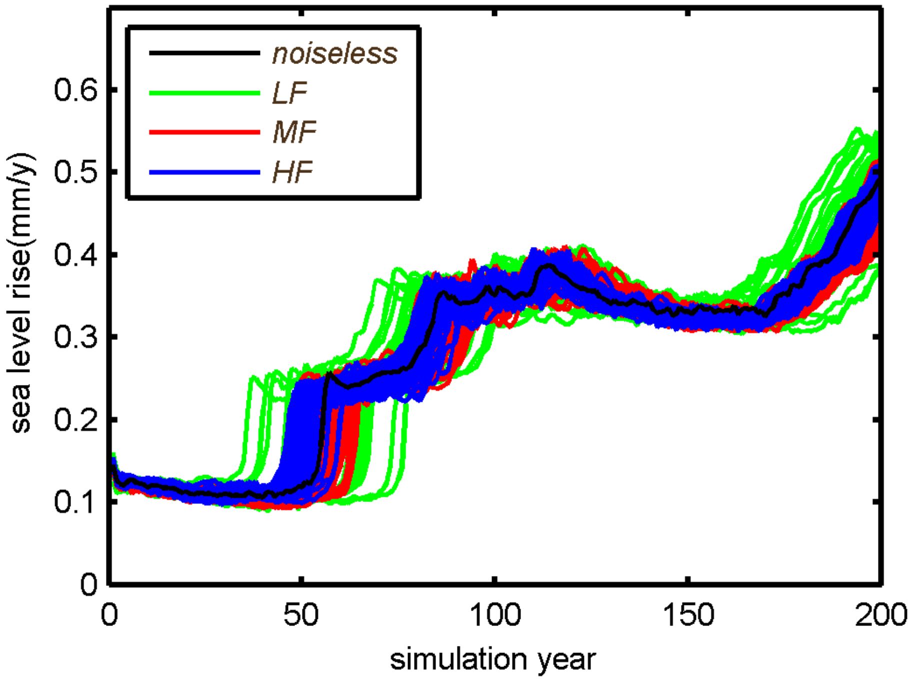

Fig. 6. Sea level rise equivalent retreating rate of Pine Island Glacier with lower (green), medium (red) and higher frequency (blue) bed rock noise. The noiseless control (black line) lies in the middle of the simulations.

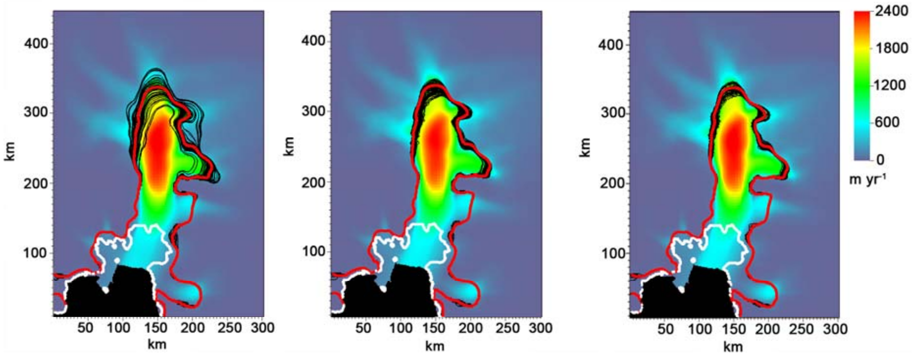

Fig. 7. Location of PIG grounding lines (first simulation year in white, last in black) and the ice velocity magnitude in the last simulation year for (left to right) lower, medium and higher frequency noise experiments. The red contour in the three plots is result of the noiseless experiment.

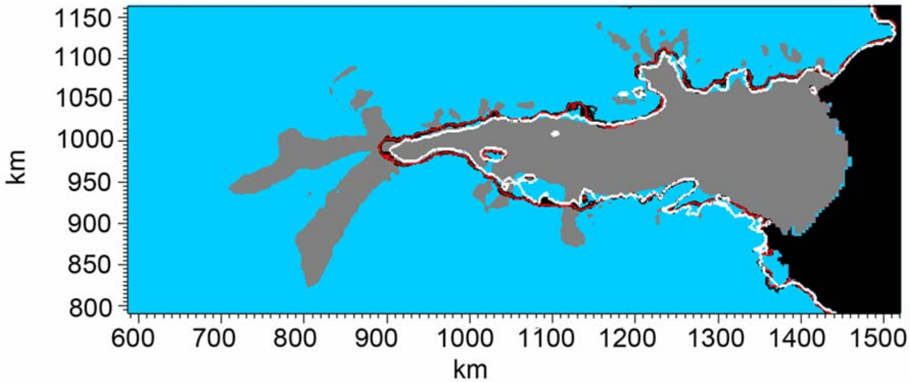

Fig. 8. Region where ice velocity > 100 m yr^{-1} (grey) for the Lambert–Amery basin (the boxed region in Fig. 2b). The location of grounding lines (first simulation year in white, last in black) in each of the 50 realizations of the low frequency noise experiments. Noiseless experiment (red contour) results are nearly coherent with these contours.

TCD
8, 479–508, 2014

Dynamic response of Antarctic ice shelves to bedrock uncertainty

S. Sun et al.

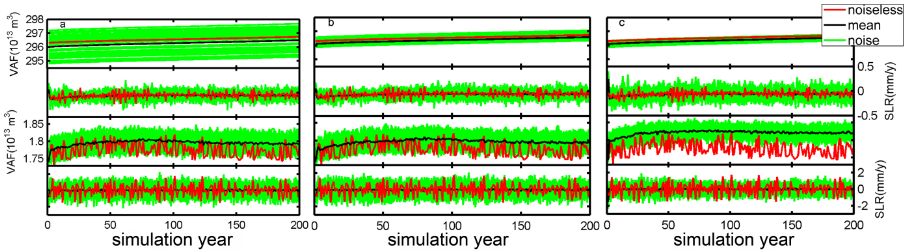

Fig. 9. Top row shows plots of ice volume above floatation (VAF) in the whole Lambert–Amery system (Fig. 1, Fig. 2b) with corresponding sea level rise (SLR) equivalent retreating rate (second row). The bottom two rows are VAF and SLR in the fast flowing part of Lambert–Amery system (grey area in Fig. 8). The three columns are for experiments with lower **(a)**, medium **(b)** and higher **(c)** frequency noise on the bedrock. The red curve is for noiseless result, green curves represent the results with noise added and the black line is the mean value of each set of results. The mean value of VAF is higher than the noiseless experiment, especially in the result with higher frequency noise.

TCD
8, 479–508, 2014

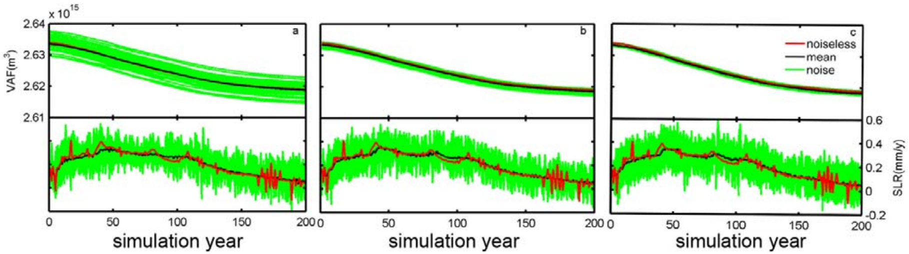

Fig. 10. As for Fig. 9 but for the Totten–Denman region (Figs. 1 and 2c).

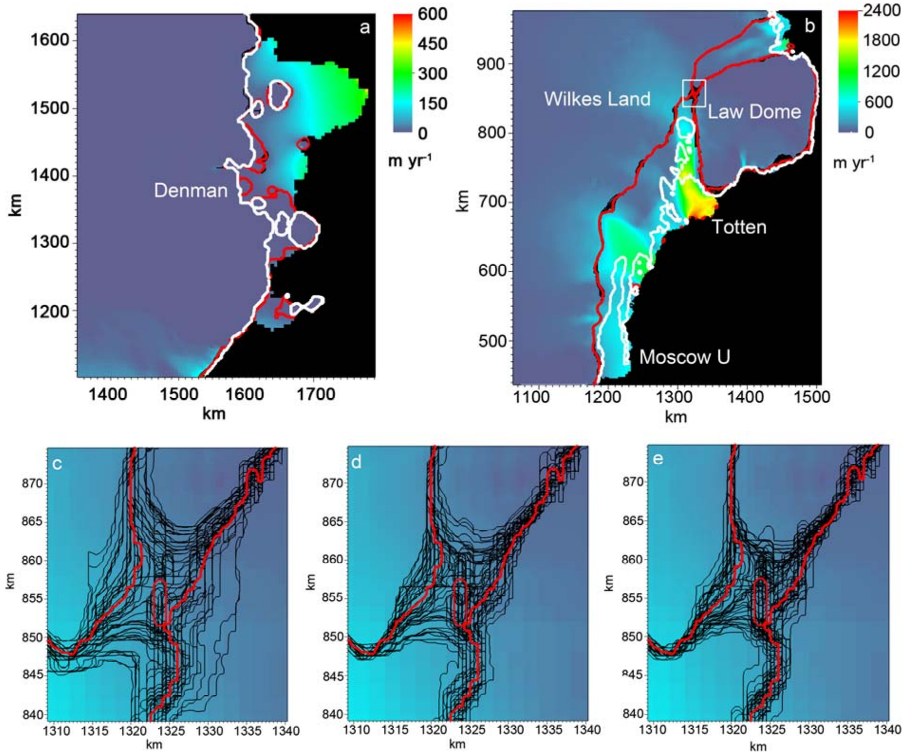

Fig. 11. (a–b) Location of Denman and Totten ice shelf grounding lines (first simulation year in white, last in black) and the magnitude of ice velocity in the final simulation year. **(c–e)** Zoom of the boxed area in **(b)**. Location of grounding line in the last simulation year for (left to right) lower, medium and higher frequency noise experiments. The red contour in the three plots is the result from the noiseless experiment.

TCD
8, 479–508, 2014